Tunnel-Barrier Rectifiers for Optical Nantennas

I. Z. Mitrovic[a], A. D. Weerakkody[a], N. Sedghi[a], S. Hall[a], J. F. Ralph[a],
J. S. Wrench[b], P. R. Chalker[b], Z. Luo[c], S. Beeby[c]

[a] Department of Electrical Eng. & El., University of Liverpool, L69 3GJ, UK
[b] Department School of Engineering, University of Liverpool, L69 3GH, UK
[c] Department of Electronics & El. Eng., University of Southampton, SO17 1BJ, UK

We present comprehensive experimental and theoretical work on tunnel-barrier rectifiers comprising double (Nb_2O_5-Al_2O_3) and triple (Ta_2O_5-Nb_2O_5-Al_2O_3) insulator configurations engineered to enhance low-voltage nonlinearity. The key rectifier properties, asymmetry, nonlinearity and responsivity have been assessed from current-voltage measurements. A superior low-voltage asymmetry (12 at 0.1 V) and responsivity (5 A/W at 0.2 V) for MIIIM rectifiers have been observed. The results demonstrate enhanced rectification by atomically multi-layering tunnel barriers in cascaded and non-cascaded MIIIM arrangements, for inclusion in optical nantennas.

Introduction

Thin film metal-insulator-metal (MIM) rectifiers using double (1-5), triple (6) or quadruple (5) insulator layers are currently the focus of attention for the development of next-generation antenna-coupled infrared (IR) detectors (7) and optical nantennas for IR energy harvesting (8). The interest is driven by their nanoscale footprint, room temperature operation, zero bias voltage requirement, and ease of integration with Complementary Metal Oxide Semiconductor technology. Highly asymmetric and nonlinear current-voltage (IV) behavior at low applied voltages is critical for these applications. The operation of a MIM device is based on quantum mechanical tunneling through a thin insulating film positioned between two metal electrodes. Hence, the operation speed of MIM devices depends on the tunneling transmission time, typically in the range of femto seconds or less, and theoretically can reach to a few 100 THz or even into the range of the solar spectrum (9). Figures of merit for MIM rectifiers include the asymmetry, nonlinearity, and turn-on voltage. These are generally limited by the work function difference that can be achieved between the metal electrodes, the barrier heights at either interface, and the mechanism of charge transport through the insulator. The choice of insulator is critical. The insulators with large electron affinities are desirable since they can produce small energy barriers at the metal electrodes and allow Fowler-Nordheim tunneling (FNT) to occur at small applied bias (low turn-on voltage). Wide band gap insulators provide high turn-on voltage. Narrow band gap insulators, such as Ta_2O_5 or Nb_2O_5, are thus attractive since small metal/insulator barrier heights allow for low turn-on voltage. For stable, temperature insensitive, high-speed operation, conduction through the insulator should be dominated by tunneling (10).

An electron tunneling device consisting of a series of laterally indented potential barriers has been proposed (11) to exhibit two distinct electron tunneling mechanisms: resonant tunneling (RT) and direct tunneling (DT). By analogy, an electron tunneling device consisting of double (MIIM) and triple (MIIIM) insulator layers has been envisaged to exhibit high asymmetry and nonlinearity (3,6). The quality of the ultra-thin (< 5 nm) insulator layers is of paramount importance; in particular, the tunnel-barrier device performance is limited by the ability to fabricate and precisely control the thickness across the entire area of the device tunnel junction through deposition process. Only recently, has this been achieved by atomic layer deposition (ALD) (3,6,12). The highest reported rectification parameters for MIIM devices based on Cr/Al_2O_3-HfO_2/Cr are: asymmetry 10 @ 3 V and responsivity < 2.5 A/W for the voltage range 0.5 - 2.5 V (3). A responsivity of 11 A/W at 0.02 V has been predicted from simulations on 4 nm resonant tunneling W/Nb_2O_5-Ta_2O_5/W diodes, however not experimentally demonstrated (4). Even, for bi-layer Ta_2O_5/Al_2O_3 MIIMs with dissimilar metal electrodes of work function difference of 0.6 eV, the highest reported low-voltage (<0.8 V) asymmetry is 10 (1,2,5). In the most recent work on Ni/NiO-ZnO/Cr, the asymmetry of 16 @ 0.5 V and responsivity of 8 A/W at 0.25 V have been reported (13). We have recently reported superior values of low-voltage asymmetry (18 @ 0.35 V) and responsivity (9 A/W @ 0.2 V) for Al/Ta_2O_5-Al_2O_3/Al and Al/Nb_2O_5-Al_2O_3/Al MIIM devices respectively (14). For MIIIM device based on Cr/Cr_2O_3-HfO_2-Al_2O_3/Cr, no asymmetry and nonlinearity values have been reported for voltages < 0.5 V (6).

In this paper, we present comprehensive experimental and theoretical work on tunnel-barrier rectifiers comprising double (Al/Nb_2O_5-Al_2O_3/Al) and triple (Al/Ta_2O_5-Nb_2O_5-Al_2O_3/Al) insulator configurations engineered to enhance low-voltage nonlinearity. The double and triple tunnel barrier structures were fabricated using atomic layer deposition. The key rectifier properties, asymmetry, nonlinearity and responsivity have been assessed from IV measurements. The results demonstrate enhanced rectification by atomically multi-layering tunnel barriers in cascaded and non-cascaded MIIIM arrangements, for inclusion in optical nantennas.

Device Fabrication and Experimental Details

The double and triple layer tunnel-barrier devices were fabricated on 4 cm × 4 cm and 2.5 cm × 2.5 cm cleaned Corning glass substrates respectively with an rms surface roughness of 0.32 nm. Surface roughness was extracted by both variable angle spectroscopic ellipsometry (VASE) and atomic force microscopy (AFM), with the tolerance of ± 0.07 nm. Then, 60 nm thick Al metal electrodes were deposited by thermal evaporation using an evaporation rate of 0.4 nm/s and defined either by photolithography or shadow mask. The rms surface roughness after Al evaporation was 0.87 nm. The surface roughness of the substrate and the bottom Al contact was found to have a large impact on device performance in agreement with recent work (15). The thin insulator (1-5 nm) layers were deposited by atomic layer deposition using a Cambridge/Nanotech Savannah reactor with water and relevant precursors such as TMA (trimethilaluminium), $Ta(OEt)_5$ (tantalum ethoxide) and $Nb(OEt)_5$ (niobium ethoxide) for Al_2O_3, Ta_2O_5 and Nb_2O_5 respectively. The precursors were heated to secure transport into the reactor; pulse and purge times were selected to ensure a self-limiting ALD reaction occurred, and the substrate temperature was maintained at 200 °C. The precursor was pulsed for 0.2 s

followed by a purge time of 4-10 s. Next, H_2O was pulsed for 0.04 s followed by a purge time of 4-10 s. This ALD cycle was continued until the desired thickness was achieved. The ALD growth per cycle (in nm/cycle) was 0.043 for Ta_2O_5, 0.04 for Nb_2O_5 and 0.125 for Al_2O_3. Note that due to breaking vacuum immediately after depositing bottom Al electrode, there was an unintentional growth of native AlO_x layer prior deposition of Ta_2O_5 (or Nb_2O_5) films. Room temperature VASE measurements were performed in the energy range 0.7–5.1 eV at three incident angles 65°, 70° and 75°, to maximize accuracy in extracting the thickness and optical constants. The reference 4 nm and 10 nm Ta_2O_5, Nb_2O_5 and Al_2O_3 films were deposited on Si, to ascertain the optical properties and band gap (14,16) by VASE, and band line-up by x-ray photoelectron spectroscopy (17). To study the quality of deposited insulator films, the reference single insulator MIM devices with nominal 4 nm Ta_2O_5 (or Nb_2O_5) films were processed. Since, the MIIM and MIIIM devices in this work were fabricated using 1 nm (nominal) Al_2O_3, and the tunneling has been found to be the dominant conduction mechanisms in Al_2O_3 layers (18), no MIM based on Al_2O_3 were considered. Room and temperature dependent (293–373 K) current voltage measurements were performed in a dark probe station, using an Agilent B1500 semiconductor parameter analyzer.

Conduction in Reference MIM Devices

Figure 1 shows experimental temperature dependent current density (J) vs voltage (JV) characteristics, for Al/Ta_2O_5/Al MIM devices processed by ALD using shorter (4 s, Fig. 1(a)) and longer (10 s, Fig. 1(b)) purge times. Less temperature dependent JV characteristic are a signature of the dominance of tunneling conduction and can be observed for the Ta_2O_5 layer in Fig. 1(b) when longer purge time was used. Nevertheless, Poole-Frenkel (PF) and Schottky emission (SE) conduction were investigated for the device processed using 4 s purge time, to determine if tunneling remained a dominant conduction in this device too. It has been reported recently that 5 nm Ta_2O_5-based MIM devices show electrode-limited SE in the low bias regime and bulk-limited PF at larger biases (19), limiting their high frequency applications. A possible solution is to introduce bi-layer of Al_2O_3 and Ta_2O_5 (1), where transport in Al_2O_3 films is dominated by tunneling (1,18), while in Ta_2O_5 by PF emission. In this case, the rectifier performance has been enhanced by a mechanism termed as “defect enhanced direct tunneling” (1).

The referring PF and SE plots for Ta_2O_5 MIM devices in this study are shown in Figs. 1(c) and (d) respectively. The relative dynamic permittivity extracted from the PF plots over the electric field range of 0-2.5 $MVcm^{-1}$ shown in Fig. 1(c), ranged from 25.6 to 39. The dielectric constant associated with PF is expected to have the high frequency value as emission of electrons from the traps should occur at times corresponding to optical frequencies. The optical permittivity has been estimated to be ~4.5 at the wavelength of 580 nm from VASE (14, 16,19), therefore from 0-2.5 $MVcm^{-1}$ PF in Ta_2O_5 is excluded as the dominant conduction mechanism. The dynamic permittivity of Ta_2O_5 extracted from SE plots in Fig. 1(d) varied from 5.1 to 2.6 with the increase in temperature from 293 K to 373 K, being comparable to the optical value. Schottky barrier height was extracted from Arrhenius plots (16) and found to be between 0.66 eV to 1.08 eV with the increase in electric field from 1.25 $MVcm^{-1}$ to 5 $MVcm^{-1}$ respectively. This could be due to the presence of both tunneling and SE at low electric fields (< 2.5 $MVcm^{-1}$).

Theoretical approximations for tunneling and thermionic emission were considered and compared with the experimental results in Fig. 1(a). The dynamic permittivity (5.1) and the barrier height (0.66 eV) extracted from fitting the experimental results to Schottky conduction in Fig. 1(d) were used for theoretical estimate of current density in Fig. 1(e). Direct tunneling and Fowler-Nordheim currents were calculated for different barrier heights at the Al/Ta_2O_5 interface as shown in Fig. 1(e).

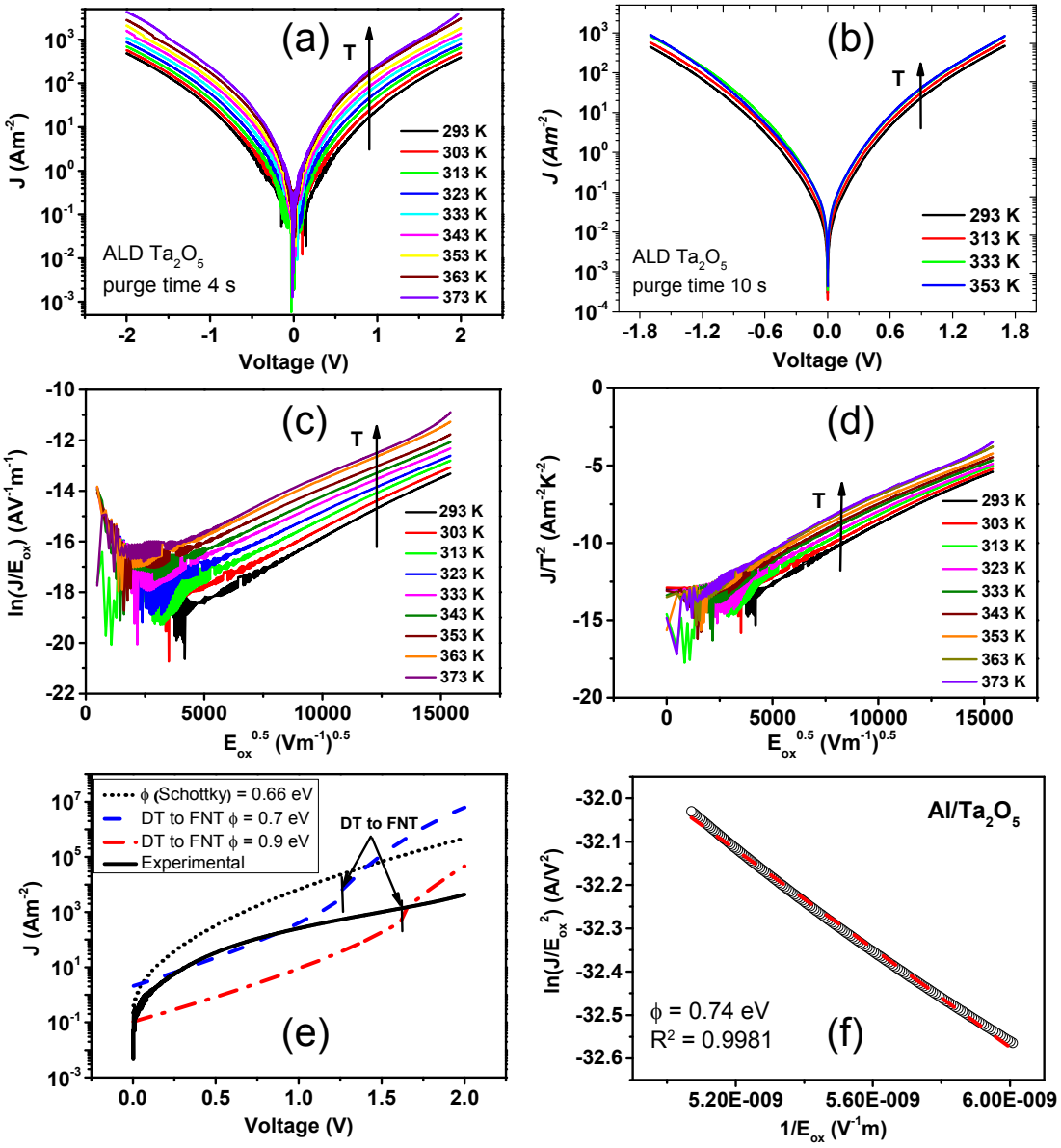

Figure 1. Experimental temperature dependent JV plots of MIM diodes with 4 nm Ta_2O_5 deposited by ALD with a purge time of (a) 4 s, (b) 10 s; (c) Poole-Frenkel and (d) Schottky emission plots from the characteristics shown in (a); (e) Fitting of the room temperature experimental JV curve with SE, DT and FNT equations using different Al/Ta_2O_5 barrier heights. (f) Estimation of the Al/Ta_2O_5 barrier height from FNT plot.

It is evident from Fig. 1(e) that the theoretically calculated current level using the Schottky equation is significantly larger than the experimentally obtained current. It can

be seen that direct tunneling with an Al/Ta_2O_5 barrier height of 0.7 eV is comparable to the experimental current at lower electric fields (0 – 2.5 $MVcm^{-1}$). The theoretical result for the Al/Ta_2O_5 barrier height of 0.7 eV in Fig. 1(e) is in agreement with the experimentally determined barrier of 0.74 eV from the FNT plot in Fig. 1(f).

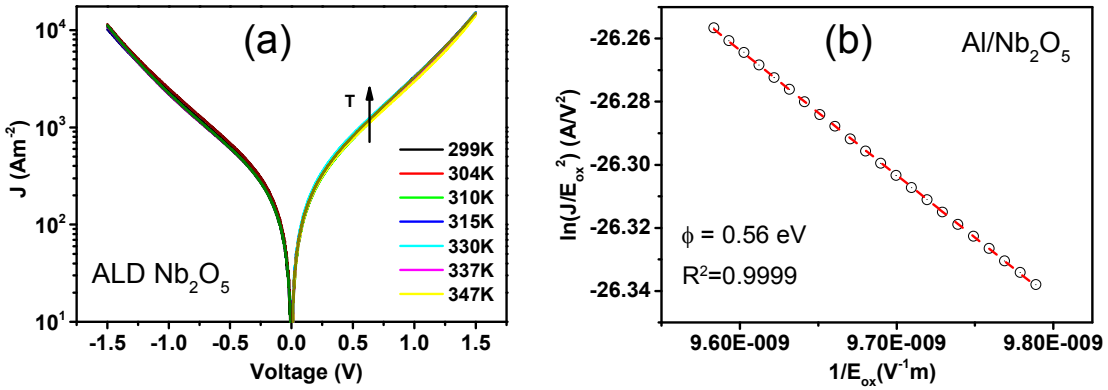

Figure 2. (a) Temperature dependent JV characteristics of MIM diode with 4 nm Nb_2O_5 deposited by ALD with a purge time of 10 s. (b) Extraction of the Al/Nb_2O_5 barrier height from FNT plot.

Figure 2(a) shows negligible temperature dependence of experimental JV curves for Al/Nb_2O_5/Al device, being a signature of tunneling as the dominant mechanism. Furthermore, the Al/Nb_2O_5 barrier height was extracted from the FNT plot in Fig. 2(b) and found to be 0.56 eV.

MIIM Tunnel-Barrier Rectifiers

Theoretical Considerations

We have previously reported (20) theoretical calculations using the multi-barrier transmission matrix method (TMM), that predict that 1 nm of Al_2O_3 and 3-6 nm of Ta_2O_5 or Nb_2O_5 using Al, can bring optimum low-voltage rectification performance. Hence, these thicknesses were used as nominal values for depositing insulators by ALD. The modified multi-barrier Tsu-Esaki method is used to calculate the current whereby the insulator stack is assumed to consist of multiple slices of the oxide with different barrier heights. The transmission amplitude at each energy level is found by solving the time-independent Schrödinger equation using TMM. The measured band alignments for 4:1 (in nm) Al/Ta_2O_5-Al_2O_3/Al and Al/Nb_2O_5-Al_2O_3/Al devices (17) are shown in Figs. 3(a) and (c) respectively. The theoretical IV curves derived using TMM for both structures are shown in Figs. 3(b) and (d). Note higher order of magnitude current for Nb_2O_5-based MIIM due to smaller barrier height of Al/Nb_2O_5. Also, the rectification reversal point (when positive bias current starts dominating negative bias current) shifts to a smaller voltage of 1.2 V for this device, in comparison to ~1.5 V for Ta_2O_5-based MIIM.

The band diagrams of the Nb_2O_5-based MIIM are shown in Fig. 4. There are two mechanisms that allow MIIM rectifiers to have a high nonlinearity while keeping the resistance low: (i) use of resonant tunneling of electrons through a quantum well formed

between the two insulators. This occurs when the metal Fermi level on the higher barrier side is biased positive creating a right-triangular well at the interface of the two insulators (Fig. 4(c)). When an allowed energy level in the quantum well aligns with the metal Fermi level on the negative side, it causes a sharp turn-on of the rectifier; (ii) use of step tunneling occurs for the opposite bias polarity, when an abrupt increase in current occurs, when the metal Fermi level on the higher barrier side rises above the conduction band (CB) of the lower barrier, thereby decreasing the tunnel distance (Fig. 4(e)). In a particular device, the choice of insulator materials, metals and thicknesses determines the mechanism that dominates.

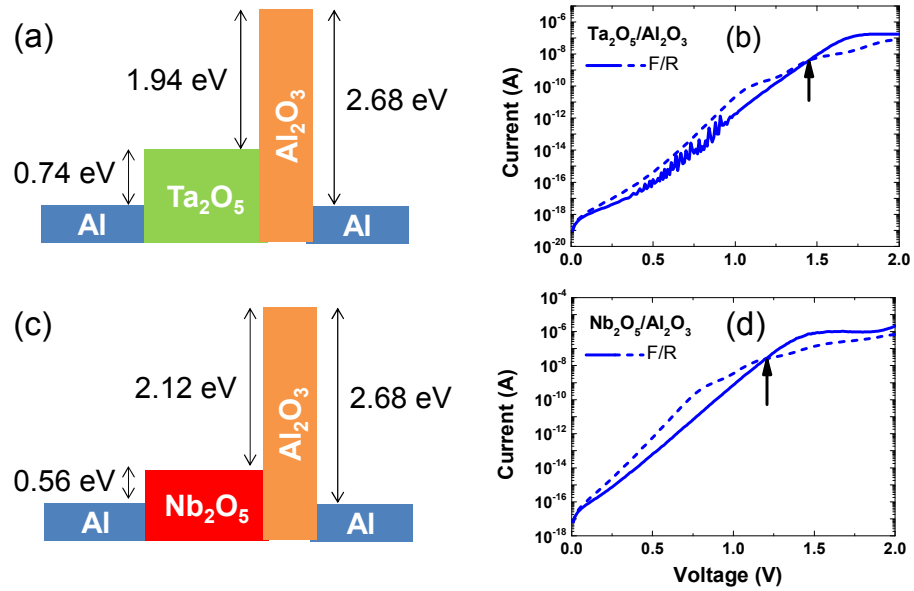

Figure 3. Measured barrier heights and theoretical IV characteristics of two MIIM diodes with Al electrodes, fabricated in this work: (a)-(b) 4 nm Ta_2O_5/1 nm Al_2O_3; (c)-(d) 4 nm Nb_2O_5/1 nm Al_2O_3. The arrows in (b) and (d) refer to rectification reversal point, where forward current (F, full line) starts dominating reverse current (R, dashed line).

There is a large CB offset between Nb_2O_5/Al_2O_3 of 2.12 eV, leading to the generation of bound states between left and right boundaries of the deep triangular quantum well with the applied field (Figs. 4(a)-(c)). It has been shown in the previous section that the conduction in Nb_2O_5 thin layers is dominated by tunneling. Therefore when the applied bias is smaller than 0.9 V (Fig. 4(a)), the electrons transport via direct tunneling mechanism. It is worth mentioning that a bound state exists at the voltage of 0.45 V in the CB of Nb_2O_5, however the number of electrons which can tunnel through at this energy level is very small due to Fermi-Dirac statistics. An onset of strong resonance can be expected if: (i) bound states are created in the quantum well of the CB of Nb_2O_5, (ii) transmitted and reflected electron wave functions are in phase, and (iii) sufficient number of electrons is injected into the structure from the metal at the energy level of bound states. For voltages around 1 V in Fig. 4(b) FNT occurs. With further increase in voltage > 1.2 V, the conditions are met for strong resonance. We have observed RT at 1.5 V for fabricated Al/Ta_2O_5-Al_2O_3/Al (14), as theoretically predicted in Fig. 3(b). Furthermore, for rf sputtered Al/Nb_2O_5-Al_2O_3/Al device, the rectification reversal was observed at ~1.1 V (14). The conduction in reverse bias up to -0.9 V is dominated by DT and FNT as

depicted in Fig. 4(d). When the applied potential is smaller than -0.9 V, the metal Fermi level is above the CB of Nb_2O_5 leading to enhanced current due to ST (Fig. 4(e)).

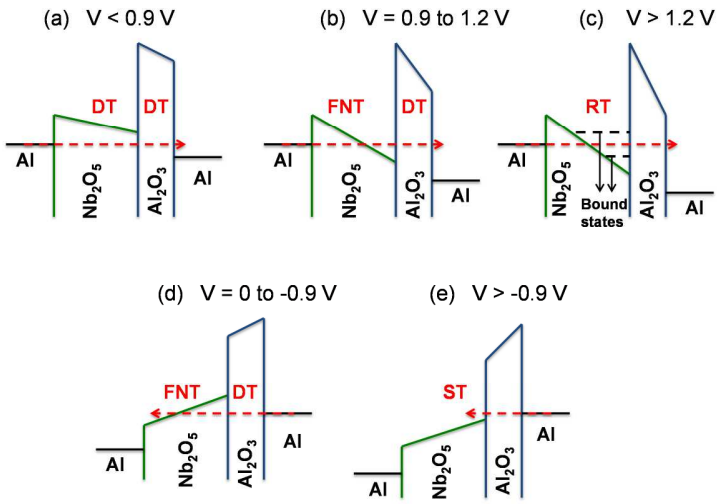

Figure 4. Energy band diagrams of Al/1 nm Al_2O_3-4 nm Ta_2O_5/Al MIIM tunnel barrier rectifier depicting different conduction mechanisms being dependent on external bias: (a)-(c) positive voltages; (d)-(e) negative voltages. DT, FNT, ST, and RT refer to direct, Fowler-Nordheim, step and resonant tunneling, respectively.

Experimental Rectification Properties

The large signal rectification is ascribed to the device asymmetry defined as the ratio of current at positive (I_+) or negative (I.) bias, whichever larger, to that at opposite bias

$$\eta_{asym} = |I_+/I_-| \text{ or } |I_-/I_+| . \qquad [1]$$

Small signal rectification, however, is governed by nonlinearity around the operating point and is usually realized by square law rectification. A measure of small signal nonlinearity is responsivity, defined as the ratio of dc rectified current, I_{dc} to input ac power, P_{in} (21)

$$Resp = \frac{I_{dc}}{P_{in}} = \frac{1}{2}\frac{I''}{I'}\bigg|_{V_p} = \frac{1}{2}\frac{dg_d/dV}{g_d} \qquad [2]$$

where I' and I'' are the first and second derivatives of current and g_d is dynamic conductance at operating point V_p. A nonlinearity factor has been defined (3) as the ratio of dynamic to static conductance i.e.

$$\chi = \frac{dI/dV}{I/V} , \qquad [3]$$

with the rate of change in nonlinearity, to reflect the small signal nonlinearity.

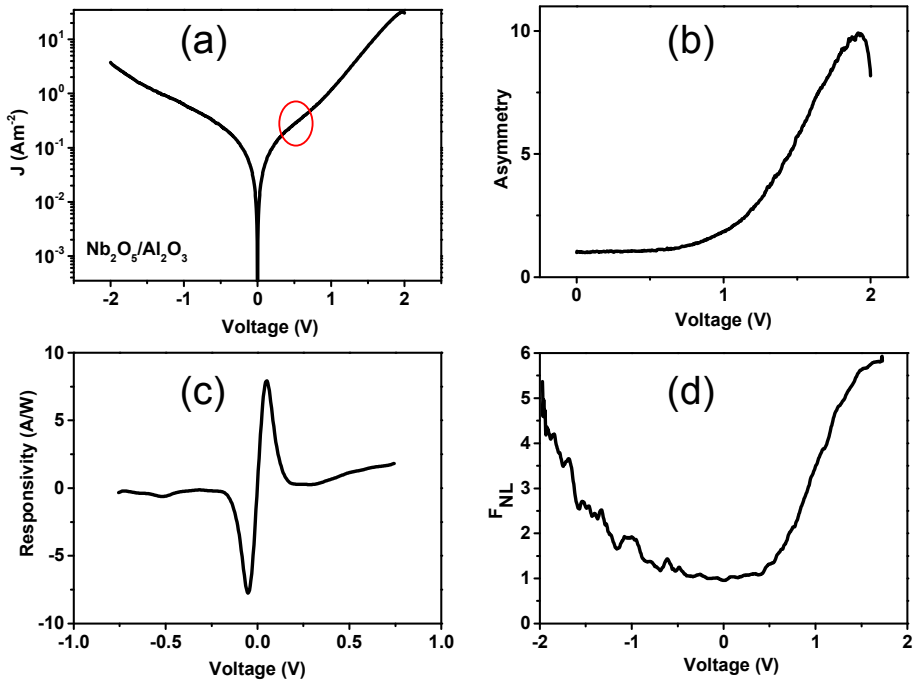

Figure 5. (a) Experimental JV results for Al/Nb_2O_5-Al_2O_3/Al tunnel diode fabricated by ALD, with nominal thickness ratio of 4:1, and its rectification properties: (b) asymmetry, (c) responsivity and (d) nonlinearity. Note that the actual Nb_2O_5 thickness measured by VASE is 4.5 nm giving the rectification reversal at 0.6 V (see the circle in (a)).

A fingerprint of resonant tunneling can be found from a change of curvature and significant increase of current in JV characteristics. A larger current for positive bias is evident for Al/Nb_2O_5/Al_2O_3/Al device shown in Fig. 5(a) from voltages > 0.6 V. The experimental value for rectification reversal is smaller than the theoretically predicted in Fig. 3(d). This result indicates that the thickness of Nb_2O_5 is larger (4.5 nm measured by VASE) than theoretically anticipated 4 nm, hence the field applied on Nb_2O_5 becomes larger resulting in the depth of the triangular quantum well to be increased. The strong resonance is then reached at lower external bias. The large signal asymmetry determined as $|I_+/I_-|$ is shown in Fig. 5(b). A peak device asymmetry of 10 can be seen at 1.9 V. The peak responsivity and nonlinearity values are found to be 7.8 A/W at 0.06 V (Fig. 5(c)) and 5.8 at 1.7 V (Fig. 5(d)) respectively.

MIIIM Tunnel-Barrier Rectifiers

Four MIIIM structures were fabricated: three in non-cascaded configuration Al-Ta_2O_5-Nb_2O_5-Al_2O_3-Al (Fig. 6(a)) by varying the insulator thicknesses (in nm) from 1:3:1, 1.5:2.5:1 and 2:2:1, and one in cascaded configuration Al-Nb_2O_5-Ta_2O_5-Al_2O_3-Al (Fig. 6(b)) with thickness ratio (in nm) 1:3:1. The measured barrier heights (17) and line-up at zero bias are depicted in Fig. 6.

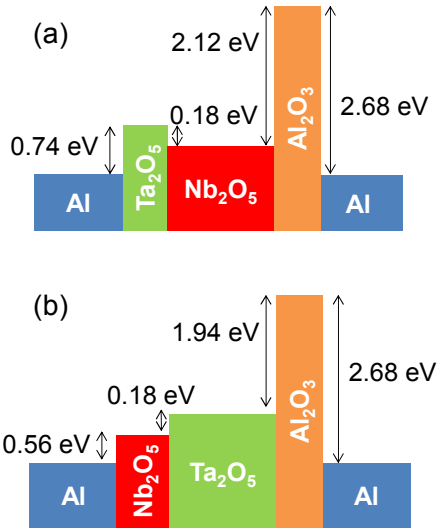

Figure 6. Measured band line-up for MIIIM barrier rectifiers fabricated in this work: (a) non-cascaded; (b) cascaded. The insulator thickness ratio for the non-cascaded Ta_2O_5-Nb_2O_5-Al_2O_3 structure varied from 1:3:1, 1.5:2.5:1 and 2:2:1, and for the cascaded Nb_2O_5-Ta_2O_5-Al_2O_3 was 1:3:1.

Non-Cascaded MIIIM Rectifiers

The energy band diagrams for MIIIM 1:3:1 configuration, are shown in Fig. 7. As seen in Fig. 7(a), even when the applied voltage is zero, there is a bound state formed in the CB of Nb_2O_5. This is due to the barriers between Nb_2O_5 and Ta_2O_5 (0.18 eV), and Nb_2O_5 and Al_2O_3 (2.12 eV). Although there is another bound state created at the potential of 0.25 V, current levels obtained is small (Fig. 8(a)), due to number of electrons which can tunnel through at this energy level is very small. However if the potential is increased above 0.35 V (Fig. 7 (b)), it is possible to observe enhanced current due to resonance.

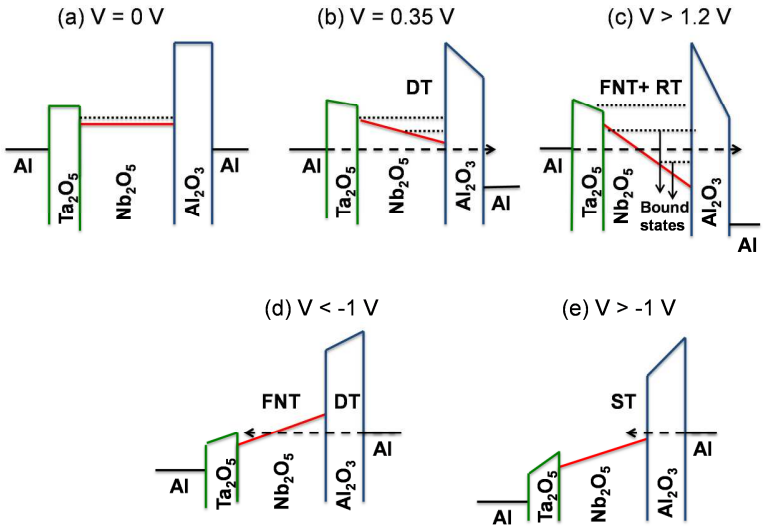

Figure 7. Band line-up for non-cascaded Ta_2O_5-Nb_2O_5-Al_2O_3 rectifier with thickness ratio 1:3:1, under (a)-(c) positive bias, (d)-(e) negative bias.

This is evident in the experimental results in Fig. 8(a). For further increase of the bias to 1.2 V (Fig. 7(c)), Nb_2O_5 reaches FNT and RT regime.

For the 1.5:2.5:1 MIIIM structure, the Nb_2O_5 thickness is smaller, hence the voltage for strong resonance to occur is higher (rectification reversal shifts to 0.4 V), while Nb_2O_5 reaches FNT sooner, at 1.1 V. Note significantly lower current for this device in Fig. 8(a) in comparison to 1:3:1 MIIIM structure. The effect of enhanced current due to resonance is less pronounced due to the smaller Nb_2O_5 thicknesses, which leads to a reduction in the portion of potential applied on it. Therefore a larger voltage must be applied to increase the depth of the triangular quantum well.

For 2:2:1 MIIIM structure, there is no evidence of observing rectification reversal at lower voltages as in previous configurations. The magnitude of reverse bias current is always larger than that of the forward bias current (Fig. 8(a)). The number of bound states remains the same up to 0.7 V for this structure, leading to the conduction to be dominated by DT. At 1.7 V, the FNT occurs. A change in curvature of the forward bias current and also a decrease in slope are visible in the experimental JV curve in Fig. 8(a) at voltages ~ 1.8 V.

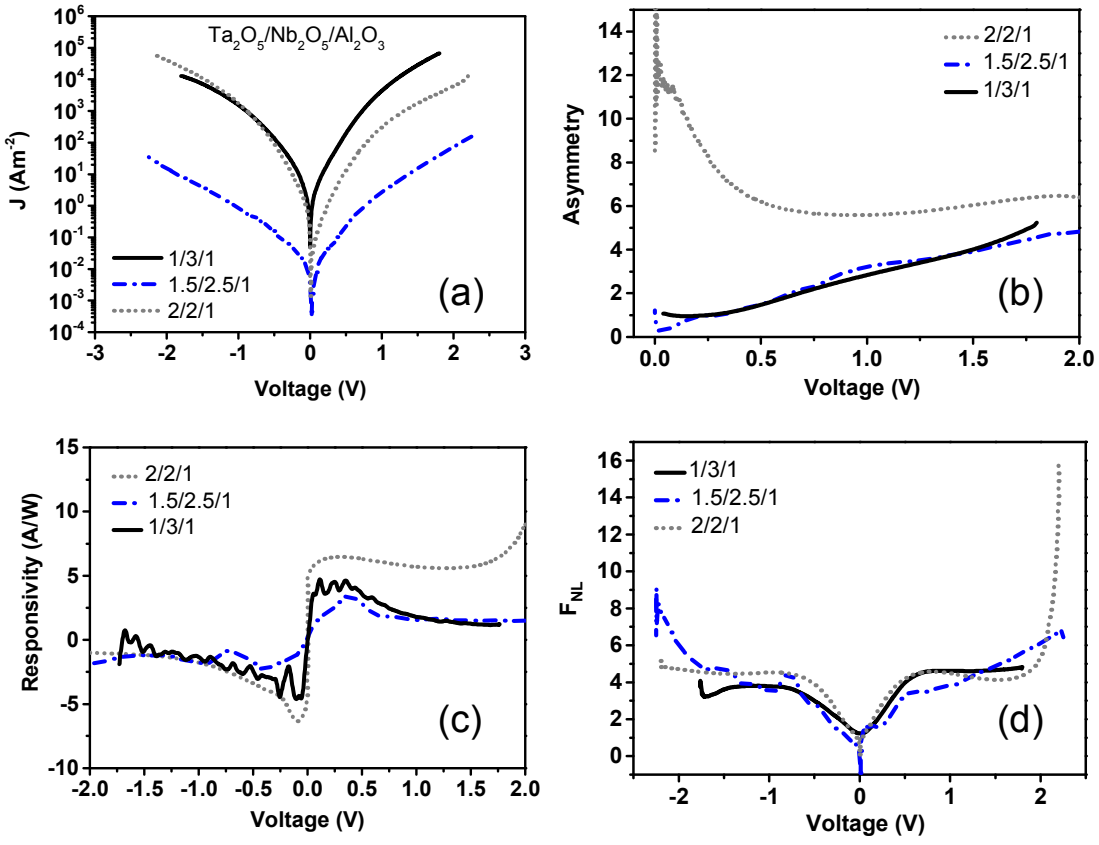

Figure 8. (a) Experimental JV characteristics for non-cascaded MIIIM tunnel rectifiers with Ta_2O_5-Nb_2O_5-Al_2O_3 thicknesses (in nm): 1:3:1, 1.5:2.5:1 and 2:2:1 fabricated by ALD; their rectification parameters: (b) asymmetry, (c) responsivity and (d) nonlinearity.

For reverse bias, the behavior is very similar for all three MIIIM configurations. The conduction in the films is dominated by DT when the applied bias is less than -1 V (Fig. 7(d)). A quantum well is created in the conduction band of Nb_2O_5 due to band bending. However, as a result of the small barrier between Nb_2O_5 and Ta_2O_5 (0.18 eV), the bound state leaks to the left, resulting in the conduction in reverse bias to be dominated solely by DT and FNT. A potential of ~ -1 V must be applied for the metal Fermi level to overcome CB of Ta_2O_5 and Nb_2O_5 to reach ST regime (Fig. 7(e)).

Asymmetry, responsivity and nonlinearity graphs for the MIIIM devices are shown in Fig. 8(b), (c) and (d) respectively. Only for the 2:2:1 MIIIM device, asymmetry is calculated by considering the ratio of reverse bias current to the forward bias current. The peak device asymmetry and responsivity values are summarized in Table 1. The highest low-voltage values were obtained for 2:2:1 MIIIM configuration with asymmetry of 12 at 0.1 V, and responsivity of 5.1 A/W at 0.24 V.

Cascaded MIIIM Rectifiers

As seen in Figure 6(b), no bound states exist in the cascaded structure for zero bias. The conduction process is dominated by DT in all three insulators if the applied bias is < 1.1 V (Fig. 9(a)). However beyond 1.1 V, it is possible to obtain a bound state in the conduction bands of both Nb_2O_5 and Ta_2O_5 (Fig. 9(b)) leading to enhanced current due to resonance. In Fig. 10(a), the rectification reversal is observed around 1 V. The strong resonance is depicted for this structure from 1.7 V (Fig. 9(c)). For reverse bias, the conduction below -1.3 V is dominated by DT and FNT (Fig. 9(d)); further decrease of voltage < -1.3 V leads to ST regime (Fig. 9(e)). Fig. 10 shows JV results for cascaded 1:3:1 MIIIM device and their rectification parameters. The device asymmetry is significantly larger in comparison to the non-cascaded MIIIM devices, with maximum value of 117 at 1.6 V. The peak responsivity is comparable, and ~5 A/W at 1 V.

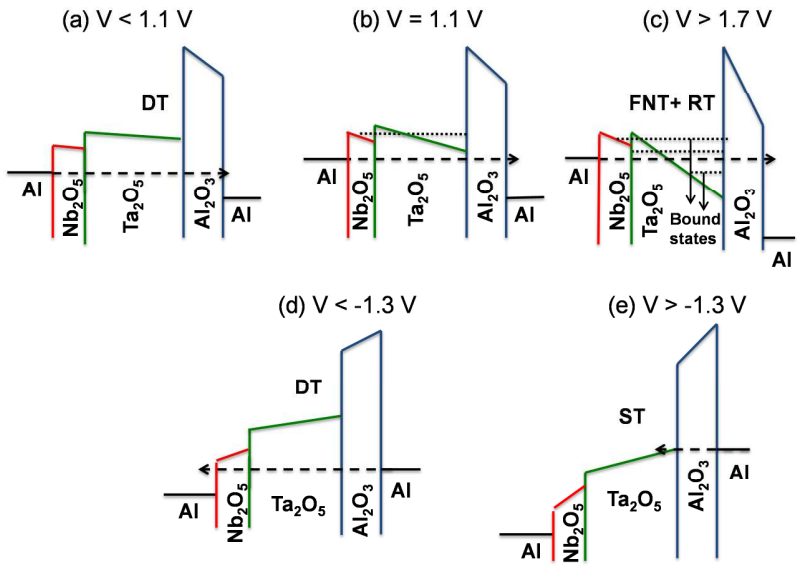

Figure 9. Energy band diagrams for cascaded MIIIM tunnel rectifier fabricated by ALD with Nb_2O_5-Ta_2O_5-Al_2O_3 thickness ratio (in nm) 1:3:1 under (a)-(c) positive bias, (d)-(e) negative bias.

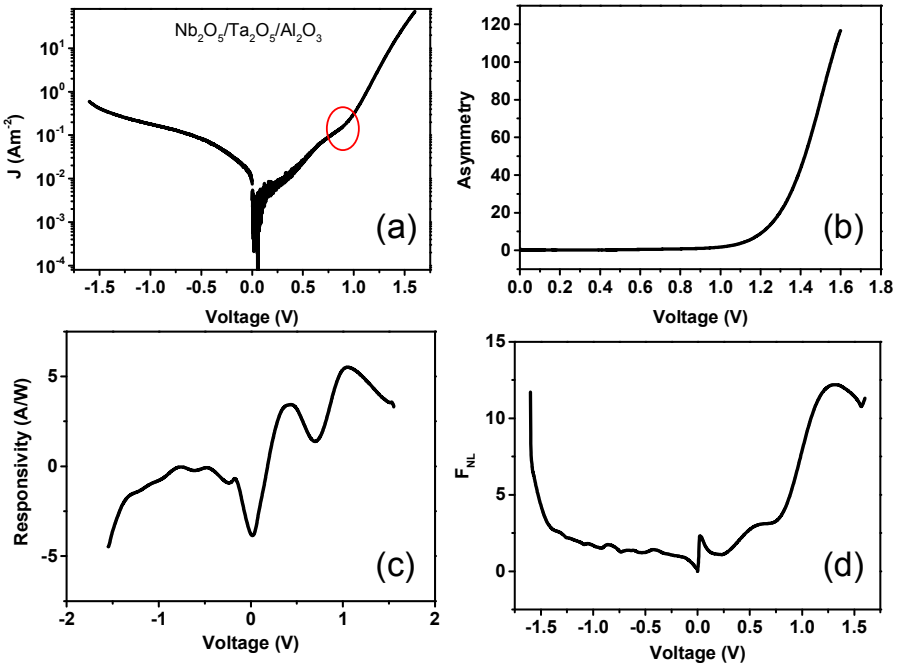

Figure 10. (a) Experimental JV characteristics for cascaded MIIIM rectifier with Nb_2O_5-Ta_2O_5-Al_2O_3 with thickness ratio (in nm) 1:3:1, its rectification properties: (b) asymmetry, (c) responsivity; (d) nonlinearity. The circle in (a) marks rectification reversal point.

In summary, the experimental peak values of asymmetry and responsivity obtained from MIIM and MIIIM devices in this work are shown in Table I.

TABLE I. A Summary of rectification parameters for ALD MIIM and MIIIM devices in this work.

Tunnel-barrier device	Asymmetry	Responsivity (A/W)
Ta_2O_5-Al_2O_3 (14)	18 @ 0.35 V	6 @ 0.1 V
Nb_2O_5-Al_2O_3	10 @ 1.9 V	7.8 @ 0.1 V
Ta_2O_5-Nb_2O_5-Al_2O_3 1:3:1	5.3 @ 1.8 V	4.3 @ 0.35 V
Ta_2O_5-Nb_2O_5-Al_2O_3 1.5:2.5:1	4.8 @ 2 V	3.4 @ 0.4 V
Ta_2O_5-Nb_2O_5-Al_2O_3 2:2:1	12 @ 0.1 V	5.1 @ 0.24 V
Nb_2O_5-Ta_2O_5-Al_2O_3 1:3:1	117 @ 1.6 V	5 @ 1 V

Summary

We demonstrate experimentally, enhanced asymmetry and low-voltage nonlinearity in ALD nanometer scale double and triple tunnel-barrier rectifiers. In-depth electrical characterization and theoretical analysis shows dominance of tunneling in thin (< 5 nm) insulator layers of Ta_2O_5 and Nb_2O_5. The Ta_2O_5-Al_2O_3 and Nb_2O_5-Al_2O_3 MIIM devices as well as the non-cascaded Ta_2O_5-Nb_2O_5-Al_2O_3 with three different thickness ratios, and a cascaded Nb_2O_5-Ta_2O_5-Al_2O_3 MIIIM device were fabricated and investigated. A fingerprint of resonant tunneling can be found from a change of curvature and significant increase of current in JV characteristics. The resonant tunneling was experimentally observed at ~0.6 V for MIIM devices, at ~0.35 V for non-cascaded MIIIM and ~ 1 V for cascaded MIIIM. Although the strong resonance had an impact on enhanced forward

biased current levels and increased asymmetry at higher voltages, the highest low-voltage asymmetry and responsivity were observed for non-cascaded MIIIM with thickness ratio (in nm) 2:2:1 where the effect of direct and step tunneling dominate current transport.

Acknowledgments

The work was funded by the EPSRC, UK, project number EP/K018930/1.

References

1. N. Alimardani and J. Conley Jr., *J. Appl. Phys.* **105**, 082902 (2014).
2. N. Alimardani and J. F. Conley, Jr., *Appl. Phys. Lett*. **102,** 143501 (2013).
3. P. Maraghechi, A. Foroughi-Abari, K. Cadien, and A. Y. Elezzabi, *Appl. Phys. Lett.* **99**, 253503 (2011).
4. S. Grover and G. Moddel, *Solid-State Electron*. **67**, 94 (2012).
5. F. Aydinoglu, M. Alhazmi, B. Cui, O. M. Ramahi, M. Irannejad, A. Brzezinski, and M. Yavuz, *J. N. Nanotechnol*. **1**, 3 (2014).
6. P. Maraghechi, A. Foroughi-Abari, K. Cadien, and A. Y. Elezzabi, *Appl. Phys. Lett.* **100**, 113503 (2012).
7. M. N. Gadalla, M. Abdel-Rahman, and A. Shamim, *Scient. Rep*. **4**, 4270 (2014).
8. S. Grover and G. Moddel, *IEEE J. Photov*. **1**, 78 (2011).
9. S. Hall, I.Z. Mitrovic, N. Sedghi, Y.C. Shen, Y. Huang, J.F. Ralph, in *Functional Nanomaterials and Devices for Electronics, Sensors and Energy Harvesting*, A. Nazarov, F. Balestra, V. Kilchytska, D. Flandre, Editors, p. 241, Springer (2014).
10. S. Krishnan, E. Stefanakos and S. Bhansali, *Thin Solid Films* **516**, 2244 (2008).
11. M. Di Ventra, G. Papp, C. Coluzza, A. Baldereschi, P.A. Schulz, *J. Appl. Phys*. **80**(7), 4174 (1996).
12. E.W. Cowell III, N. Alimardani, C.C. Knutson, J.F. Conley Jr, D.A. Keszler, B.J. Gibbons, J.F. Wager, *Adv. Mater.* **23**, 74 (2011).
13. A. Singh, R. Ratnadurai, R. Kumar, S. Krishnan, Y. Emirov, S. Bhansali, *Appl. Surf. Sci.* **334**, 197 (2015).
14. A.D. Weerakkody, N. Sedghi, I.Z. Mitrovic, H. van Zalinge, I. Nemr Noureddine, S. Hall, J.S. Wrench, P.R. Chalker, L.J. Phillips, R. Treharne, K. Durose, *Microelectronic Eng.* **147**, 298 (2015).
15. N. Alimardani, E. W. Cowell, J. F. Wagner, J. F. Conley, D. R. Evans, M. Chin, S. J. Kilpatrick, M. Dubey, *J. Vac. Sci. Technol A*. **30**, 01A113 (2012).
16. A.D. Weerakkody, N. Sedghi, X. Zhan, I.Z. Mitrovic, S. Hall, Proc. IEEE PRIME, p. 133 (2015).
17. I.Z. Mitrovic, A.D. Weerakkody, N. Sedghi, S. Hall, J. Ralph, J.S. Wrench, P.R. Chalker, Z. Luo, S. Bebby, *Appl. Phys. Lett*. (2016) (in preparation)
18. N. Alimardani, S.W. King, B.L. French, C. Tan, B.P. Lampert, J.F. Conley Jr., *J. Appl. Phys*. **116**, 024508 (2014).
19. N. Alimardani, J. McGlone, J.F. Wager, J.F. Conley Jr., *J. Vac. Sci. Tech. A*, **32**, 01A122 (2014).
20. N. Sedghi, J. W. Zhang, J. F. Ralph, Y. Huang, I. Z. Mitrovic, and S. Hall, Proc. ESSDERC, p. 131 (2013); N. Sedghi, J. F. Ralph, I.Z. Mitrovic, P. R. Chalker, S. Hall, *Appl. Phys. Lett.* **102**, 092103 (2013).
21. T.C.L.G. Sollner, W.D Goodhue, P.E. Tannenwald, C.D Parker and D.D. Peck, *Appl. Phys. Lett*. **43**, 588 (1983).